Assessing Reciprocity in Polarimetric SAR Data

Augusto Aubry, *Senior Member, IEEE*, Vincenzo Carotenuto, *Senior Member, IEEE*, Antonio De Maio, *Fellow, IEEE*, Luca Pallotta, *Senior Member, IEEE*

***Abstract*— This letter studies the conformity with the reciprocity theorem on measured polarimetric SAR data. The problem is formalized via a binary hypothesis test where the reciprocity assumption is tested versus its alternative (absence of reciprocity). The Generalized Likelihood Ratio (GLR) is used as design criterion and the resulting decision rule ensures the Constant False Alarm Rate (CFAR) property. At the analysis stage, the performance of the GLR statistic is analyzed on simulated data as well as on two different measured datasets (collected by two systems) thus highlighting the effectiveness of the approach.**

***Index Terms*— Polarimetric SAR, reciprocity, covariance matrix.**

I. Introduction

In monostatic backscattering scenarios, where the transmit and receive antennas are co-located, the polarimetric scattering matrix, also known as the Sinclair matrix, is defined as [1, eq. (3.15)]

$$\boldsymbol{S} = \begin{pmatrix} S_{\text{HH}} & S_{\text{HV}} \\ S_{\text{VH}} & S_{\text{VV}} \end{pmatrix}$$

whereby the S_{XY} entry is the complex scattering return for X transmit polarization and Y receive polarization. For targets/media whose internal state is unaltered by the polarization of the transmit signal, the reciprocity theorem requires that the two cross-polar terms are equal, i.e., $S_{\text{HV}} = S_{\text{VH}}$ and enforces a symmetric structure to $\boldsymbol{S}$. This is expected to be the case for most natural scatterers even if real data might not always exactly comply with the reciprocity theorem due to statistical fluctuations, Faraday rotations [2], as well as measurement errors related to channel mismatches and sensor non idealities. To circumvent this drawback, calibration procedures can be used as for instance those summarized in [3, Sections 13-15]. The calibrated image is then used for polarimetric processing applications such as coherent change detection, classification, etc. [1], [4]–[15], assuming that reciprocity holds true. In fact, only three channels are usually processed (possibly the cross-channel is computed as the coherent average of the HV and VH returns [16]). In this respect it would be of interest to develop a statistical test aimed at ascertaining to what extent the polarimetric scattering matrix of a pixel in a calibrated SAR image complies with the reciprocity condition. This is indeed the scope of this study which formulates the compliance with reciprocity as a binary hypothesis test where the reciprocity (H_0) is tested versus its alternative (i.e., lack of reciprocity, H_1), with a given confidence level represented by the type-I error of the test (i.e., false alarm probability P_{FA}). The problem is solved resorting to the Generalized Likelihood Ratio Test (GLRT) and the performance of the technique is assessed on simulated data as well as on real recorded SAR data collected by two different systems with different hardware and operating frequency.

The remainder of the letter is organized as follows: Section II is devoted to problem formulation and GLRT derivation, whereas Section III describes the conducted analyses as well as the obtained results. Finally, Section IV draws some conclusions.

Augusto Aubry and Antonio De Maio are with Dipartimento di Ingegneria Elettrica e delle Tecnologie dell'Informazione, Università "Federico II", via Claudio 21, I-80125 Napoli, Italy. E-mail: augusto.aubry@unina.it, ademaio@unina.it.

Vincenzo Carotenuto and Luca Pallotta are with CNIT udr Università "Federico II", via Claudio 21, I-80125 Napoli, Italy. E-mail: vincenzo.carotenuto@unina.it, luca.pallotta@unina.it.

Notation

The adopted notation uses boldface for vectors $\boldsymbol{a}$ (lower case), and matrices $\boldsymbol{A}$ (upper case). The transpose, conjugate, and conjugate transpose are denoted by $(\cdot)^T$, $(\cdot)^*$, and $(\cdot)^\dagger$, respectively. $\text{tr}\{\cdot\}$ and $\det(\cdot)$ are the trace and the determinant of the square matrix argument, respectively. $\boldsymbol{I}$ indicates the identity matrix, $\boldsymbol{1}$ is a vector of all 1 entries, and $\boldsymbol{0}$ is a vector of all 0 entries, whose sizes are determined from the context. Finally, the letter j represents the imaginary unit ($j = \sqrt{-1}$).

II. Problem Formulation and Proposed Solution

A Quad-Pol SAR sensor, for each pixel of the image under test, measures $N = 4$ complex returns collected from four different polarimetric channels. The N returns associated with the same pixel are organized in the specific order HH, VV, HV, and VH to form the vector $\boldsymbol{x}_{l,m}$, $l = 1, \ldots, L$ and $m = 1, \ldots, M$ (L and M are the vertical and horizontal size of the image), therefore, a 3-D data stack of size $M \times L \times N$ is available. For the generic pixel under test, a rectangular neighbourhood $\mathcal{A}$ of size $K = W_1 \times W_2 \geq N$ is extracted, and the vectors within it are indicated as $\boldsymbol{x}_1, \ldots, \boldsymbol{x}_K$.

The polarimetric returns $\boldsymbol{x}_1, \ldots, \boldsymbol{x}_K$ are modeled as independent and identically distributed (i.i.d.) zero-mean circularly symmetric complex Gaussian vectors whose covariance matrix is $\boldsymbol{M}_1$ in the presence of a generic non-reciprocal medium and $\boldsymbol{M}_0$ when a reciprocal medium is considered. To discern between the occurrence of reciprocity and its alternative, the following binary hypothesis test is defined:

$$\begin{cases} H_0 : \text{reciprocity} \\ H_1 : \text{non-reciprocity} \end{cases} \tag{1}$$

Under the H_0 hypothesis, the covariance is structured as:

$$\boldsymbol{M}_0 = \begin{pmatrix} \bar{\boldsymbol{M}} & \begin{matrix}\delta & \delta\\ \delta_1 & \delta_1\end{matrix} \\ \begin{matrix}\delta^* & \delta_1^* \\ \delta^* & \delta_1^*\end{matrix} & \sigma^2\mathbf{1}\mathbf{1}^\dagger \end{pmatrix} + \gamma^2\boldsymbol{I}, \tag{2}$$

where $\bar{\boldsymbol{M}}$ is a 2×2 Hermitian positive semidefinite matrix and γ^2 accounts for the thermal noise power level. The first term stems from the observation that under the reciprocity assumption the covariances of the entries in

$$[S_{\text{HH}},\, S_{\text{VV}},\, S_{\text{HV}},\, S_{\text{VH}}] = [S_{\text{HH}},\, S_{\text{VV}},\, S_{\text{HV}},\, S_{\text{HV}}],$$

which coincide with the correlations due to the zero-mean assumption, satisfy

$$\begin{aligned}\mathbb{E}\left[|S_{\text{HV}}|^2\right] &= \mathbb{E}\left[|S_{\text{VH}}|^2\right] = \mathbb{E}\left[S_{\text{HV}}S_{\text{VH}}^\dagger\right] \\ &= \mathbb{E}\left[S_{\text{VH}}S_{\text{HV}}^\dagger\right] = \sigma^2,\end{aligned} \tag{3}$$

$$\mathbb{E}\left[S_{\text{HH}}S_{\text{HV}}^\dagger\right] = \mathbb{E}\left[S_{\text{HH}}S_{\text{VH}}^\dagger\right] = \delta, \tag{4}$$

and

$$\mathbb{E}\left[S_{\text{VV}}S_{\text{HV}}^\dagger\right] = \mathbb{E}\left[S_{\text{VV}}S_{\text{VH}}^\dagger\right] = \delta_1. \tag{5}$$

Introducing the unitary matrix $\boldsymbol{U}$

$$\boldsymbol{U} = \begin{pmatrix} \boldsymbol{I} & \mathbf{0} & \mathbf{0} \\ \mathbf{0}^T & 1/\sqrt{2} & 1/\sqrt{2} \\ \mathbf{0}^T & 1/\sqrt{2} & -1/\sqrt{2} \end{pmatrix}, \tag{6}$$

it is possible to transform $\boldsymbol{M}_0$ in a block diagonal matrix, i.e.,

$$\begin{aligned}\boldsymbol{U}\boldsymbol{M}_0\boldsymbol{U}^\dagger &= \begin{pmatrix} \boldsymbol{I} & \mathbf{0} & \mathbf{0} \\ \mathbf{0}^T & 1/\sqrt{2} & 1/\sqrt{2} \\ \mathbf{0}^T & 1/\sqrt{2} & -1/\sqrt{2} \end{pmatrix} \\ &\begin{pmatrix} \bar{\boldsymbol{M}} & \begin{matrix}\delta & \delta\\ \delta_1 & \delta_1\end{matrix} \\ \begin{matrix}\delta^* & \delta_1^* \\ \delta^* & \delta_1^*\end{matrix} & \sigma^2\mathbf{1}\mathbf{1}^\dagger \end{pmatrix} \begin{pmatrix} \boldsymbol{I} & \mathbf{0} & \mathbf{0} \\ \mathbf{0}^T & 1/\sqrt{2} & 1/\sqrt{2} \\ \mathbf{0}^T & 1/\sqrt{2} & -1/\sqrt{2} \end{pmatrix} + \gamma^2\boldsymbol{I} \\ &= \begin{pmatrix} \tilde{\boldsymbol{M}} & \mathbf{0} \\ \mathbf{0}^T & \gamma^2 \end{pmatrix},\end{aligned} \tag{7}$$

where $\tilde{\boldsymbol{M}}$ is a 3×3 Hermitian positive definite matrix.

To solve Problem (1), we resort to the GLRT, whose expression is given by

$$\frac{\max\limits_{\boldsymbol{M}_1} f\left(\boldsymbol{r}_1, \boldsymbol{r}_2, \ldots, \boldsymbol{r}_K | \boldsymbol{M}_1, H_1\right)}{\max\limits_{\boldsymbol{M}_0} f\left(\boldsymbol{r}_1, \boldsymbol{r}_2, \ldots, \boldsymbol{r}_K | \boldsymbol{M}_0, H_0\right)} \underset{H_0}{\overset{H_1}{\gtrless}} \eta, \tag{8}$$

with η a suitable threshold and $f\left(\boldsymbol{r}_1, \boldsymbol{r}_2, \ldots, \boldsymbol{r}_K | \boldsymbol{M}_h, H_h\right)$ the likelihood under the H_h hypothesis, $h = 0, 1$. The expression of the maximum likelihood under H_1 hypothesis can be derived as

$$\begin{aligned}&\max_{\boldsymbol{M}_1} f\left(\boldsymbol{r}_1, \boldsymbol{r}_2, \ldots, \boldsymbol{r}_K | \boldsymbol{M}_1, H_1\right) \\ &\quad= \max_{\boldsymbol{M}_1} \frac{1}{\pi^{NK}[\det(\boldsymbol{M}_1)]^K} \exp\left\{-\text{tr}\left(\boldsymbol{S}_0\boldsymbol{M}_1^{-1}\right)\right\} \\ &\quad= \frac{c_{N,K}}{[\det(\boldsymbol{S}_0)]^K},\end{aligned} \tag{9}$$

where $c_{N,K}$ is a constant and $\boldsymbol{S}_0 = \sum_{i=1}^K \boldsymbol{x}_i\boldsymbol{x}_i^\dagger$. As to the H_0 hypothesis, the maximum likelihood can be cast as

$$\begin{aligned}&\max_{\boldsymbol{M}_0} f\left(\boldsymbol{r}_1, \boldsymbol{r}_2, \ldots, \boldsymbol{r}_K | \boldsymbol{M}_0, H_0\right) \\ &\quad= \max_{\boldsymbol{M}_0} \frac{1}{\pi^{NK}[\det(\boldsymbol{M}_0)]^K} \exp\left\{-\text{tr}\left(\boldsymbol{S}_0\boldsymbol{M}_0^{-1}\right)\right\} \\ &\quad= \max_{\tilde{\boldsymbol{M}},\gamma} \frac{1}{\pi^{NK}[\det(\tilde{\boldsymbol{M}})]^K\gamma^{2K}} \exp\left\{-\text{tr}\left(\boldsymbol{S}_{c1}\tilde{\boldsymbol{M}}^{-1}\right)\right\} \\ &\quad\quad \exp\left\{-S_{c2}\gamma^{-2}\right\} \\ &\quad= \frac{c_{N,K}}{[\det(\boldsymbol{S}_{c1})]^K S_{c2}^K},\end{aligned} \tag{10}$$

where

$$\boldsymbol{S}_1 = \boldsymbol{U}\boldsymbol{S}_0\boldsymbol{U}^\dagger = \begin{pmatrix} \boldsymbol{S}_{c1} & \boldsymbol{w} \\ \boldsymbol{w}^\dagger & S_{c2} \end{pmatrix}.$$

Therefore, from the ratio of (9) and (10), the GLRT can be evaluated as

$$\frac{\det(\boldsymbol{S}_{c1})}{\det(\boldsymbol{S}_0)} S_{c2} \underset{H_0}{\overset{H_1}{\gtrless}} \eta, \tag{11}$$

with η a suitable modification of the original threshold. Now, since $\det(\boldsymbol{S}_0) = \det(\boldsymbol{S}_1)$, (11) can be also written in the following more compact form

$$\begin{aligned}\frac{\det(\boldsymbol{S}_{c1})}{\det(\boldsymbol{S}_1)} S_{c2} &= \frac{\det(\boldsymbol{S}_{c1})}{\det(\boldsymbol{S}_{c1})(S_{c2} - \boldsymbol{w}^\dagger\boldsymbol{S}_{c1}^{-1}\boldsymbol{w})} S_{c2} \\ &= \frac{S_{c2}}{(S_{c2} - \boldsymbol{w}^\dagger\boldsymbol{S}_{c1}^{-1}\boldsymbol{w})},\end{aligned} \tag{12}$$

where in the first equality, the expression of a block partitioned matrix determinant [17] is used. Finally, the GLRT can be also written in the following equivalent form

$$\frac{\boldsymbol{w}^\dagger\boldsymbol{S}_{c1}^{-1}\boldsymbol{w}}{S_{c2}} \underset{H_0}{\overset{H_1}{\gtrless}} \eta, \tag{13}$$

Two important remarks are now necessary.

A. Remark 1: CFAR Property

Observe that under H_0

$$\boldsymbol{S}_{1,w} = \begin{pmatrix} \tilde{\boldsymbol{M}}^{-1/2} & \mathbf{0} \\ \mathbf{0}^T & \gamma^{-1} \end{pmatrix} \boldsymbol{S}_1 \begin{pmatrix} \tilde{\boldsymbol{M}}^{-1/2} & \mathbf{0} \\ \mathbf{0}^T & \gamma^{-1} \end{pmatrix} \tag{14}$$

is a complex Wishart matrix with identity matrix parameter. Besides $\boldsymbol{S}_{c1,w} = \tilde{\boldsymbol{M}}^{-1/2}\boldsymbol{S}_{c1}\tilde{\boldsymbol{M}}^{-1/2}$ and $S_{c2,w} = S_{c2}/\gamma^2$.

The decision statistic at the left hand side of (12) can be written as

$$\frac{\det(\boldsymbol{S}_{c1})}{\det(\boldsymbol{S}_1)} S_{c2} = \frac{\det(\boldsymbol{S}_{c1,w})}{\det(\boldsymbol{S}_{1,w})} S_{c2,w} \tag{15}$$

and its distribution, under H_0, turns independent of $\tilde{\boldsymbol{M}}$ and γ^2 due to the identity matrix parameter of $\boldsymbol{S}_{1,w}$. Hence, the Constant False Alarm Rate (CFAR) property can be claimed.

B. Remark 2: Noise Level Estimation

If reciprocity holds true, i.e., test (13) selects the H_0 hypothesis, it is also possible to obtain directly from the matrix $\boldsymbol{S}_1$ the ML estimate of the sensor noise level based on the component S_{c2}. Specifically, $\hat{\gamma}^2 = S_{c2}/K$. This could be very useful for some additional signal processing/classification applications which can benefit from the noise level knowledge.

III. Performance Assessment

This section is devoted to the performance study of the proposed GLRT for reciprocity analysis on polarimetric SAR images. The first subsection considers a quantitative analysis on simulated data, whereas the subsequent analyzes reciprocity on measured full-polarimetric SAR data.

A. Analysis on Simulated Data

The present subsection shows the results obtained on simulated data, considering the detection probability P_D as figure of merit. Due to the lack of a closed form expression, P_D is evaluated over 10^3 Monte Carlo simulations, setting the threshold to ensure a certain nominal false alarm probability, i.e., $P_{FA} = 10^{-4}$.

Thanks to the CFAR property, the threshold is computed in the presence of white interference. Whereas, under the H_1 hypothesis, the simulated data $\boldsymbol{x}_k$, $k = 1, \ldots, K$, are modeled as zero-mean N-dimensional ($N = 4$ in this case) i.i.d. complex circular Gaussian vectors sharing the covariance matrix $\boldsymbol{M}_1 = \bar{\boldsymbol{M}}_1 + \gamma^2 \boldsymbol{I}$, i.e.,

$$\boldsymbol{x}_k \sim \mathcal{CN}(\boldsymbol{0}, \boldsymbol{M}_1), \quad k = 1, \ldots, K,$$

with $\gamma^2 = 10^{-3}$ the actual thermal noise power level and $\bar{\boldsymbol{M}}_1$ a specific $N \times N$ Hermitian matrix, associated with a scene composed of trees [4],

$$\bar{\boldsymbol{M}}_1 = 0.256 \begin{pmatrix} 1 & 0.61 & 0 & 0 \\ 0.61 & 0.89 & 0 & 0 \\ 0 & 0 & 0.16 & 0.16\,(1+\xi)\,e^{-j\phi} \\ 0 & 0 & 0.16\,(1+\xi)\,e^{j\phi} & 0.16\,(1+\xi)^2 \end{pmatrix},$$

where ξ is a scaling factor that models modulus variations, and ϕ accounts for phase mismatches between the HV and VH channels[1].

Figure 1 reports P_D versus the parameter ξ for some number of looks K of practical interest. Each subplot refers to a specific scenario in terms of phase difference among the polarimetric channels HV and VH. Precisely, ϕ is chosen for the three subplots, respectively, as: a) $\phi = 0$, b) a uniform random variable $\phi = \mathcal{U}[-5°, 5°]$, c) a uniform random variable $\phi = \mathcal{U}[-10°, 10°]$. The curves clearly show that for ξ values close to 0, the H_0 hypothesis (i.e., reciprocity) is detected, whereas moving away from that value, the H_1 hypothesis (i.e., non-reciprocity) is preferred. In addition, from the graphs it can be pointed out that an increment in the number of looks produces an always better detection for even smaller variations between the two channels. Finally, increasing the variability of ϕ (i.e., from subplot a to c), H_1 selection arises also in correspondence of $\xi = 0$, confirming the effectiveness of the test to detect phase mismatches in the cross-polarized returns.

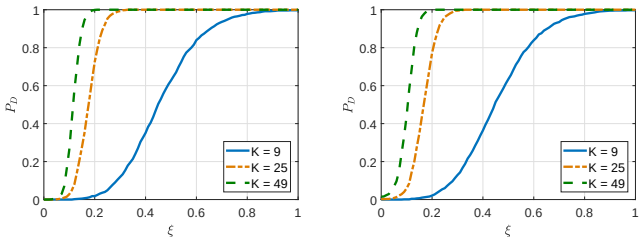

(a) (b)

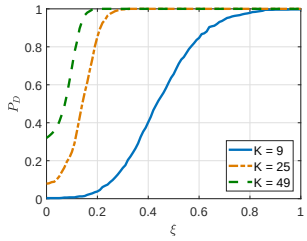

(c)

Fig. 1. P_D versus ξ for different number of looks, and perfect phase matching between the two channels HV and VH (a), random phase variation $\mathcal{U}[-5°, 5°]$ (b) and random phase variation $\mathcal{U}[-10°, 10°]$ (c). The nominal P_{FA} is set to 10^{-4}.

B. Test on Measured SAR Data

This subsection validates reciprocity on two different full-polarimetric datasets[2]:

- L-band (1.25 GHz) coherent polarimetric dataset, acquired by the fully polarimetric Danish airborne SAR system, ElectroMagnetic Institute Synthetic Aperture Radar (EMISAR) on April 17th, 1998. The image (1750×1000 pixels) represents a scene of the Foulum Area (DK), Denmark, and contains a mixed urban, vegetation and water area.
- C-band (5.30 GHz) coherent polarimetric dataset, acquired by the dual-frequency fully polarimetric Convair-580 SAR from the Canadian Centre for Remote Sensing (CCRS) on June 26th, 2001. The image (222×3429 pixels) represents a scene of Ottawa (Ontario), Canada, and contains a mixed urban and vegetation area.

[1]Note that, for $\xi = 0$ and $\phi = 0°$, the considered model is associated to a perfectly reciprocal medium.

[2]Both data can be downloaded at *https://earth.esa.int/web/polsarpro/data-sources/sample-datasets* [16].

In Figure 2, reciprocity is assessed for the Foulum EMISAR data. Precisely, the figure shows the image span[3], the modulus of the difference between the HV and VH channels, the values of the GLR computed over the image by using a sliding window of size $K = W \times W = 9$, and the results of the test exploiting a threshold evaluated for a nominal P_{FA} equal to 10^{-4}. Figure 3 is structurally equal to Figure 2, but it refers to the Ottawa Convair data. The results of these tests (subplots d) highlight that these two fully-polarimetric data can be assumed to share the reciprocity property since the number of detections (i.e., H_1 hypothesis) is very limited with respect to the overall number of analyzed pixels within images. As a matter of fact, as drawn in Table I, the percentage of pixels that do not exhibit a reciprocal behavior is only the 0.04% and 3% of the total for EMISAR and Convair data, respectively. Notice the agreement among the detection maps in Figures 2-d) - 3-d) and the $|\mathrm{HV} - \mathrm{VH}|$ values reported in 2-b) and 3-b): detections correspond to high values of $|\mathrm{HV} - \mathrm{VH}|$.

Some discussion on the results is now necessary. In this respect it is worth observing that texture changes, edges/mixed boundaries, as well as deviations from Gaussianity can trigger false decisions on reciprocity. This would suggest the use of a multistage test to assess the lack of reciprocity in the sense that, if a detection is declared, it could be necessary a confirmation via a test (possibly more sophisticated) which is robust with respect to texture variations. Besides, it could also be possible that moving toward edges/boundaries the assumption of i.i.d. looks could be violated determining a false response of the test due to data with different and possibly mixed scattering mechanisms. The last observations might allow for a possible justification of the different number of threshold crossings for the two considered datasets in that the different degree of heterogeneity in the illuminated scene probably plays an important role.

TABLE I

PERCENTAGE OF ESTIMATED PIXELS COMPLYING H_0 (NOT COMPLYING H_1) WITH RECIPROCITY ON THE REAL DATA OF FIGURES 2-3.

	L-Band EMISAR	C-Band Convair
H_0	99.96%	97%
H_1	0.04%	3%

IV. CONCLUSIONS

Reciprocity is an important assumption usually made in polarimetric SAR signal processing. This letter has considered the problem of assessing the compliance of measured polarimetric SAR data with reciprocity. In this respect a GLRT-based framework is proposed to discriminate among reciprocity and its counterpart. The decision rule ensures the CFAR property and permits the selection of a detection threshold independent of the operative environment and on the sensor characteristics. The numerical examples on simulated data has given a quantitative measurement of the effectiveness of the proposed approach. In addition, the tests on two different measured SAR data have confirmed the benefits and effectiveness of this technique.

Possible future research avenues might concern the extension of the framework to an environment where the power of the returns changes from pixel to pixel. This implies that the polarimetric covariance matrix is spatially varying and the sample covariance matrix is no longer the ML estimate.

[3]Recall that the span is defined as the power of the SAR image, i.e., the sum of the square modules of the polarimetric channels.

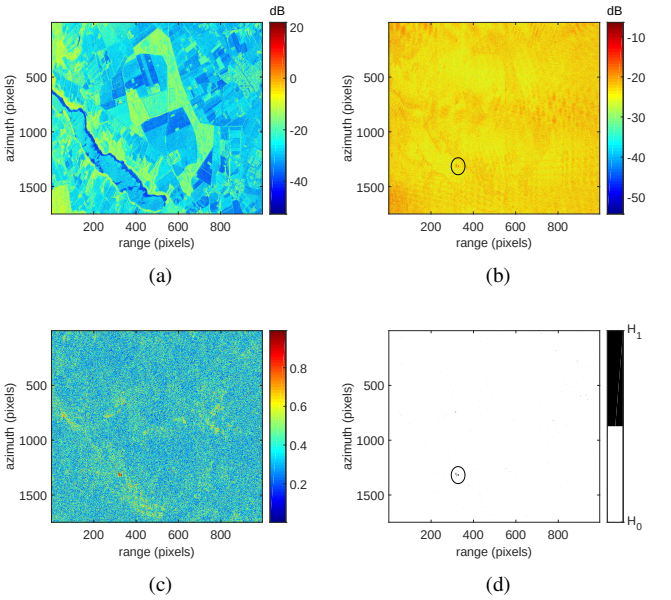

Fig. 2. Reciprocity assessment for the L-band EMISAR data of Foulum Area, DK, using $K = 9$ looks. Image span in dB (a), modulus of the difference between the HV and VH channels in dB (b), GLR statistics (c), and GLRT (d). The nominal P_{FA} evaluated on simulated white data is set equal to 10^{-4}.

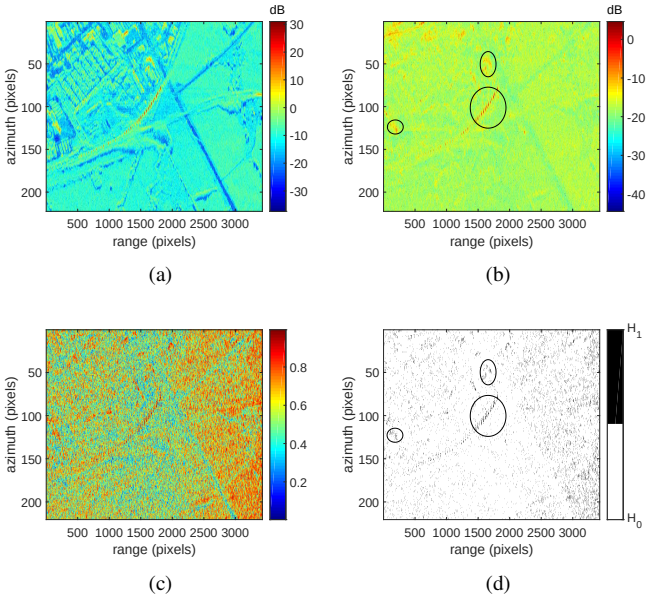

Fig. 3. Reciprocity assessment for the C-band Convair data of Ottawa Area, CA, using $K = 9$ looks. Image span in dB (a), modulus of the difference between the HV and VH channels in dB (b), GLR statistics (c), and GLRT (d). The nominal P_{FA} evaluated on simulated data is set equal to 10^{-4}.

ACKNOWLEDGMENT

The authors would like to acknowledge ESA for providing the EMISAR and Convair data.

The authors thank the Associate Editor and the Reviewers for the useful comments toward the improvement of the paper.

REFERENCES

[1] J. S. Lee and E. Pottier, *Polarimetric Radar Imaging: From Basics to Applications*, CRC Press, 2009.

[2] E. J. M. Rignot, "Effect of Faraday Rotation on L-Band Interferometric and Polarimetric Synthetic-Aperture Radar Data," *IEEE Transactions on Geoscience and Remote Sensing*, vol. 38, no. 1, pp. 383–390, January 2000.

[3] F. T. Ulaby and D. G. Long, *Microwave Radar and Radiometric Remote Sensing*, University of Michigan Press, 2013.

[4] L. M. Novak, M. C. Burl, and W. W. Irving, "Optimal Polarimetric Processing for Enhanced Target Detection," *IEEE Transactions on Aerospace and Electronic Systems*, vol. 29, no. 1, pp. 234–244, January 1993.

[5] S. R. Cloude and E. Pottier, "An Entropy Based Classification Scheme for Land Applications of Polarimetric SAR," *IEEE Trans. on Geoscience and Remote Sensing*, vol. 35, no. 1, pp. 68–78, January 1997.

[6] L. Ferro-Famil and E. Pottier (Editor in Chief J. A. Kong), *Progress In Electromagnetics Research*, vol. 24, chapter Dual Frequency Polarimetric SAR Data Classification and Analysis, pp. 251–276, New York Elsevier, 2001.

[7] L. M. Novak, "Change Detection for Multi-Polarization Multi-Pass SAR," in *Algorithms for Synthetic Aperture Radar Imagery XII*. International Society for Optics and Photonics, 2005, vol. 5808, pp. 234–247.

[8] S. E. Park, W. M. Moon, and E. Pottier, "Assessment of Scattering Mechanism of Polarimetric SAR Signal From Mountainous Forest Areas," *IEEE Trans. on Geoscience and Remote Sensing*, vol. 50, no. 11, pp. 4711–4719, 2012.

[9] A. Moreira, P. Prats-Iraola, M. Younis, G. Krieger, I. Hajnsek, and K. P. Papathanassiou, "A Tutorial on Synthetic Aperture Radar," *IEEE Geoscience and Remote Sensing Magazine*, vol. 1, no. 1, pp. 6–43, 2013.

[10] V. Carotenuto, A. De Maio, C. Clemente, J. J. Soraghan, and G. Alfano, "Forcing Scale Invariance in Multipolarization SAR Change Detection," *IEEE Transactions on Geoscience and Remote Sensing*, vol. 54, no. 1, pp. 36–50, January 2016.

[11] L. Pallotta, C. Clemente, A. De Maio, and J. J. Soraghan, "Detecting Covariance Symmetries in Polarimetric SAR Images," *IEEE Trans. on Geoscience and Remote Sensing*, vol. 55, no. 1, pp. 80–95, January 2017.

[12] D. Ciuonzo, V. Carotenuto, and A. De Maio, "On Multiple Covariance Equality Testing with Application to SAR Change Detection," *IEEE Transactions on Signal Processing*, vol. 65, no. 19, pp. 5078–5091, October 2017.

[13] L. Pallotta, A. De Maio, and D. Orlando, "A Robust Framework for Covariance Classification in Heterogeneous Polarimetric SAR Images and its Application to L-Band Data," *IEEE Trans. on Geoscience and Remote Sensing*, vol. 57, no. 1, pp. 104–119, January 2019.

[14] L. Pallotta and D. Orlando, "Polarimetric Covariance Eigenvalues Classification in SAR Images," *IEEE Geoscience and Remote Sensing Letters*, vol. 16, no. 5, pp. 746–750, May 2019.

[15] D. Yang, L. Du, H. Liu, Y. Wang, and M. Gu, "Extended Geometrical Perturbation Based Detectors for PolSAR Image Target Detection in Heterogeneously Patched Regions," *IEEE Journal of Selected Topics in Applied Earth Observations and Remote Sensing*, vol. 12, no. 1, pp. 285–301, January 2019.

[16] ESA, "PolSARPro (The Polarimetric SAR Data Processing and Educational Tool)," 2000-2019.

[17] R. A. Horn and C. R. Johnson, *Matrix Analysis*, Cambridge University Press, 1990.